ACCSCIENCE PUBLISHING

International Journal of Bioprinting

RESEARCH ARTICLE

# Bioprinting with adipose stem cells and hydrogel modified with bioactive glass

**Krishna C.R. Kolan[1], Apurv Saxena[2], Bradley A. Bromet[3], Lesa B. Steen[4], August T. Bindbeutel[1], Julie A. Semon[3]*, Delbert E. Day[4], and Ming C. Leu[1]**

[1]Department of Mechanical and Aerospace Engineering, Missouri University of Science and Technology, Rolla, Missouri, United States of America

[2]Department of Chemistry, Missouri University of Science and Technology, Rolla, Missouri, United States of America

[3]Department of Biological Sciences, Missouri University of Science and Technology, Rolla, Missouri, United States of America

[4]Department of Material Science and Engineering, Missouri University of Science and Technology, Rolla, Missouri, United States of America

## Abstract

Bioprinting research is focused on utilizing growth factors and multiple cell types to create clinically relevant three-dimensional (3D) tissue models using hydrogels. Rheological and biological challenges are two main factors that limit the creation of extrudable bioactive hydrogels. In this study, we investigate incorporation of fast dissolving and bioactive borate glass in different weight to volume percentages (0.075 to 0.6%) to alginate-gelatin (1:1) hydrogel to improve rheological properties and enable bioprinting with bioactive glass. The addition of glass improved the stiffness of the hydrogel. Human adipose-derived mesenchymal stem cells (ASCs) were uniformly mixed in this bioink at $1 \times 10^6$ cells/mL concentration, and spheroid specimens were cultured in both static and dynamic culture conditions. Grid-shaped scaffolds measuring ~$18 \times 18 \times 1$ mm$^3$ were fabricated with the viable glass concentrations, and ASC viability was evaluated using Live/Dead assay. Despite immediate toxicity, an increased viability after 7 days with 0.15 w/v % or less borate glass content demonstrated the potential in utilizing highly resorbable calcium-releasing biomaterials such as bioactive glasses to modify hydrogels suitable for bioprinting cellularized 3D structures.

***Keywords:*** Bioink; Bioactive glass; Ceramics; Adipose stem cells; Alginate; Gelatin

***Corresponding author:**
Julie A. Semon
(semonja@mst.edu)

**Citation:** Kolan KCR, Saxena A, Bromet BA, et al. Bioprinting with adipose stem cells and hydrogel modified with bioactive glass. *Int J Bioprint*. 2024;10(2):2057. doi: 10.36922/ijb.2057

**Received:** October 18, 2023
**Accepted:** January 31, 2024
**Published Online:** March 1, 2024



## 1. Introduction

Extrusion-based bioprinting is gaining in popularity because its versatility enables the fabrication of materials over a wide range of viscosities.[1] A majority of the current generation commercial bioprinters are all based on extrusion three-dimensional (3D) printing techniques.[2] The success of extrusion-based bioprinting depends largely on the proper selection of an extrudable hydrogel precursor and the proper selection of cell type. Hydrogels such as alginate, chitosan, hyaluronic acid, gelatin, collagen, fibrin, Matrigel, Pluronic® F127, and polyethylene glycol are commonly used to encapsulate

cells for extrusion-based bioprinting techniques.[3] No one material offers both the required rheological and biological properties, and therefore, it is a common practice to create a composite hydrogel to suit specific bioprinting application.

Alginate has been extensively used as synthetic extracellular matrix (ECM) that mimics native human tissues for more than three decades.[4,5] Alginate is derived from algae that crosslinks in the presence of divalent cations such as $Ca^{2+}$ and $Mg^{2+}$ and is suitable for bioprinting applications.[6] As alginate exhibits poor cell adhesion and proliferation due to the lack of arginine-glycine-aspartate (RGD) tripeptide sequences, it is functionalized to include RGD peptide sequence in its molecular structure.[7,8] An alternative approach is to add gelatin to alginate to prepare a composite hydrogel to enhance the hydrogel's ability to support cell adhesion and rheological properties for extrusion-based bioprinting techniques.[9-14] Despite being unstable at physiological temperatures, gelatin improves the printability of the composite alginate+gelatin (AG) hydrogel at room temperature due to the thermoreversible gel–sol transition behavior of gelatin.[9] AG hydrogels have been evaluated by researchers in different weight ratios to improve rheological properties at room temperature to facilitate printability without affecting the cell viability.[10,14] Researchers have also pursued media ionic strength modification and deposition at ~10°C, instead of room temperature, to improve printability.[13] Despite good viability (~90%) with epidermal stem cells, sheep stem cells, and aortic smooth muscle cells in the above studies, the main challenges that remain for AG hydrogel are to achieve: (i) printability at room temperature, (ii) controlled degradation of alginate, and (iii) slower dissolution of gelatin for improved viability over time.

Until the late 2000s, a material was considered bioactive upon formation of a hydroxyapatite-like layer on its surface to bond with hard tissue (bone) upon implantation.[15,16] Recently, the definition of "bioactive" has expanded, and the bioactive glass dissolution products have been increasingly investigated for vascularization, wound healing, cardiac, lung, and nerve tissue engineering applications in addition to traditional bone repair and teeth applications.[17] The research on bioactive glasses has evolved to produce glass compositions that are highly resorbable based on borate ($B_2O_3$) network instead of traditional silicate ($SiO_2$) network.[18-20] The dissolution of bioactive glasses depends not only on the durability of the main glass-forming network (e.g., $SiO_2$ or $B_2O_3$) and the overall glass composition, but it also depends on several other factors such as residual stresses during heat treatment and surface roughness.[21] It is known that borate glass dissolves at a faster rate compared to Bioglass®, and the calcium ($Ca^{2+}$) ions released during glass dissolution could initiate the crosslinking of alginate-based hydrogels.[22] Recently, investigators added copper or niobium to bioactive glass and then printed with hydrogel in order to fabricate a fast-recovering and printable construct.[23,24] Other researchers used borate-based bioactive glass to improve the printability of AG hydrogels by increasing the stiffness of the printed construct.[25]

Previously, we investigated cell viability in a 3D-bioprinted AG-glass composite hydrogel, using a recently FDA-approved borate-based bioactive glass (13-93B3 glass, referred to as B3) and human adipose stem cells (ASCs).[26] The B3 glass is particularly attractive due to its high dissolution rate and angiogenic ability.[27-29] This specific glass composition has demonstrated an ability to heal difficult-to-treat diabetic wounds, a capability thought to stem from their angiogenic properties. However, the exact reasons for their effectiveness and the underlying mechanisms involved are still not entirely clear. One recent study showed that an increased collagen III/collagen I ratio for ASCs with B3 glass exposure could establish one possible mechanism for wound-healing behavior with B3 glass.[30]

ASCs are extracted from the stromal vascular fraction of subcutaneous fat, which is more accessible and involving a less invasive procedure than acquiring their bone marrow counterpart, the more commonly studied bone-derived mesenchymal stem cells.[31-33] Additionally, they yield a greater number of cells after isolation than bone-derived mesenchymal stem cells and have a higher proliferative capacity. For these reasons, in addition to their differentiation, angiogenic, and therapeutic abilities, they are increasingly used in tissue engineering strategies.

In this study, we: (i) examined how the rheological characteristics of AG hydrogel are enhanced by adding B3 microparticles, (ii) identified the optimal range of B3 glass in bioprinting AG hydrogels and ASC viability, and (iii) evaluated the stability of AG hydrogel and the dissolution of gelatin under these conditions.

## 2. Materials and methods

### 2.1. Cell culture

Frozen vials of human ASCs were thawed and plated in complete cell culture media (CCM) and incubated at 37°C with 5% humidified $CO_2$. To ensure that the findings were universal and not unique to a single donor, ASCs from three different unrelated donors (LaCell, New Orleans, LA, USA) were tested in all experiments. More details about the ASC culture conditions and media requirements can be found in our previous work.[34,35] CCM was prepared with alpha minimum essential media (α-MEM) by adding 10% fetal bovine serum, 1% 100× L-glutamine, and

1% 100× antibiotic/antimycotic. On the second day of culture, ASCs were washed with phosphate-buffered saline (PBS), viable ASCs were harvested with 0.25% trypsin/1 mM ethylenediaminetetraacetic acid (EDTA), and re-plated at a concentration of no more than 15,000 ASCs per dish. ASCs that reached ≤70% confluency were lifted between the second and sixth passages for suspension in AG hydrogels for all experiments. ASCs from subsequent passages were not utilized for experiments as they could affect pluripotent properties of ASCs.

### 2.2. Bioink preparation

Gelatin (Type B, Sigma-Aldrich, St. Louis, MO, USA) in 3 w/v % (0.3 g in 10 mL) was dissolved in Dulbecco's Modified Eagle Medium (DMEM; Gibco, Thermo Fisher Scientific, MA, USA) in a glass beaker at ~40°C while being magnetically stirred at 150 rpm. After gelatin dissolution, sodium alginate (Sigma-Aldrich, St. Louis, MO, USA) in 3 w/v % (0.3 g in 10 mL) was added to the gelatin solution and mixed overnight to obtain the AG hydrogel. B3 glass powder particles (less than 20 μm with ~3 μm $d_{50}$ particle size; chemical composition in wt.%: 53% $B_2O_3$, 20% CaO, 12% $K_2O$, 6% $Na_2O$, 5% MgO, 4% $P_2O_5$) were added to the solution in four different weight ratios (0.075, 0.15, 0.3, and 0.6 w/v %) after gelatin dissolution and allowed to dissolve for ~10 min before the addition of alginate powder. For example, 0.075 w/v % B3 glass corresponds to 1.25% of total combined weight of alginate and gelatin in the solution. Therefore, AG hydrogels made with 0.075, 0.15, 0.3, and 0.6 w/v % B3 glass are referred as 1.25G, 2.5G, 5G, and 10G, respectively, in this paper. All powders including gelatin, sodium alginate, and B3 glass powder particles were ultraviolet-sterilized before being added to the DMEM solution. ASCs pellet ($4 \times 10^6$) was re-suspended in 0.2 mL CCM and pipetted into AG hydrogel and magnetically stirred for no more than 3 min to obtain a uniform cell distribution and a final ASC concentration of $1.0 \times 10^6$ cells per 1 mL of bioink. The bioink was transferred to 3 mL Loctite® Henkel syringe barrel, centrifuged to remove air bubbles, and attached with 22G (410 μm) or 25G (250 μm) tips (SmoothFlow Tapered, Nordson EFD, Westlake, OH, USA) for 3D bioprinting.

### 2.3. Rheological characterization

For rheological characterization, hydrogels were prepared in deionized (DI) water with gelatin (3 w/v %), alginate (3 w/v %), and AG (6 w/v %), and with the addition of B3 glass in different weight concentrations. AG hydrogels with and without B3 glass were tested for viscosity using a Kinexus rheometer (Malvern Panalytical, Westborough, MA, USA) with a parallel plate set-up. A gap of 0.5 mm was set between plates, and the measurements were conducted at room temperature. A fresh scoop of gel was loaded each time to test viscosity, recovery, yield strength, etc. Three different tests were conducted on the gels: (i) viscosity vs. shear rate (to measure viscosity with increasing shear rate from 0.1 to 100 $s^{-1}$), (ii) oscillation amplitude sweep, and (iii) recovery tests (changing shear rate from steady state to a predetermined rate for a certain amount of time). In oscillation amplitude sweeps, percentage strain was considered input, and machine output data of loss vs. storage modulus components were plotted. Data points below 0.1 $s^{-1}$ shear rate were not reported because of the instability at low shear rates. Although one set of data was reported for each gel type, measurements were repeated to confirm the validity of the data. Statistical analysis of the rheological data was not performed because of the significant differences between the samples prepared with several orders of magnitudes difference in results.

### 2.4. Scaffold fabrication

A custom-modified tabletop cartesian 3D printer to include syringes connected through digital syringe dispenser (Loctite®, Rocky Hill, CT, USA) was used to fabricate scaffolds. The 3D printer and printing schema are illustrated in Figure 1a and b, and the 3D printer is shown in Figure 1c. Scaffold dimensions were set to 15 mm length, 15 mm width, and ~ 1 mm thickness (6 layers) and printed with 0–90° filament orientation in alternate layers. A customized software was written for G-code generation and syringe dispenser control. Sterile practices were followed for scaffold fabrication with ASCs, bioink syringes were maintained at room temperature, and the scaffolds were bioprinted in less than an hour inside the laminar flow hood.

### 2.5. Physical assessment

Test specimens with overall dimensions of $40 \times 20 \times 5$ $mm^3$ were fabricated to have a 20 mm gauge length and 10 mm section width for tensile tests. Dense specimens without any designed pores were used for these tests, and specimens were crosslinked with 0.1 M $CaCl_2$ solution for 10 min before tensile tests. Specimens were tested on Instron machine (Instron 5969, Norwood, MA, USA) at a crosshead speed of 5 mm/min. The swelling properties of the hydrogel were assessed on scaffolds with dimensions of $15 \times 15 \times 1$ $mm^3$. Swelling percentage (S) was calculated using the formula, $S = [(S_t - S_c)/S] \times 100$, where $S_t$ is scaffold weight after 24 h soak in DI water, and $S_c$ is scaffold weight immediately after crosslinking.

### 2.6. Scanning electron microscopy

Hydrogel in bulk (~2–3 mL in a centrifuge tube) was freeze-dried to porous foam-like pellets. The pellets were coated with Au-Pd for about ~60 s by mounting the samples on a rotating platform using a Hummer Sputter Coater. The

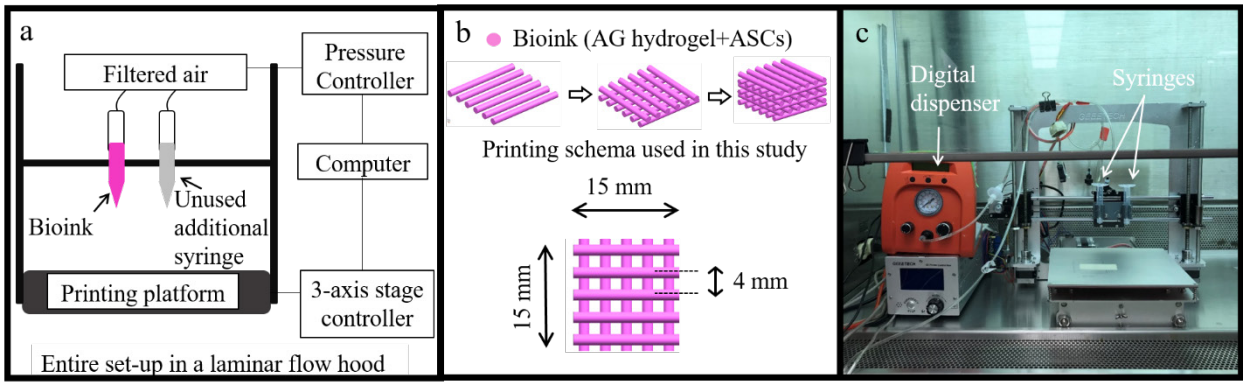


**Figure 1**. Extrusion-based 3D printing. (a) Schematic of printer used in this study; (b) the printing process and scaffold dimensions; (c) bioprinter in the laminar flow hood with a syringe dispenser.

samples were observed under a field emission scanning electron microscope (FE-SEM, S-4700, Hitachi, Japan) to analyze the microstructure by capturing the images at 5 kV accelerating voltage at various magnifications.

### 2.7. X-ray diffraction analysis

X-ray diffraction (XRD) analysis (Philips X-Pert, Westborough, MA, USA) was performed on the powdered freeze-dried sample to test for any crystalline hydroxyapatite-like formations in the material. Scans were run from 2θ values ranging from 10° to 80° using Cu Kα radiation (λ = 0.154056 nm).

### 2.8. $^1$H-NMR spectroscopy analysis

In this work, gelatin was physically blended with alginate to form a composite gel and not chemically crosslinked. It was expected that with time as bioprinted scaffold is incubated at 37°C, gelatin present in the scaffold could potentially be separated and leached into the media. In order to study the release of gelatin from the AG hydrogel used in this study, AG, 1.25G, and 2.5G scaffolds measuring 15 × 15 × 1 mm$^3$ were fabricated without cells, crosslinked with 0.1 M $CaCl_2$ solution for 10 min, and washed twice with DI water. The samples were soaked in DI water in airtight containers under standard culture conditions for up to 7 days. The surrounding DI water collected after 1 day and 7 days including the $CaCl_2$ solution used for crosslinking were all analyzed for presence of gelatin using proton nuclear magnetic resonance ($^1$H-NMR) spectroscopy (Bruker 400 MHz Avance™ III HD, Billerica, MA, USA). First, known quantities of gelatin were dissolved in DI water, and 0.2 mL of gelatin solution was mixed with 0.6 mL of deuterium oxide (99.9 atom %, Sigma Aldrich, St. Louis, MO, USA), and the solution was transferred to NMR tube (Colorspec®, Sigma Aldrich, St. Louis, MO, USA) and analyzed for 10 min. The area under a unique characteristic gelatin peak at ~1.9 ppm (Figure 2a) on the horizontal axis was calculated

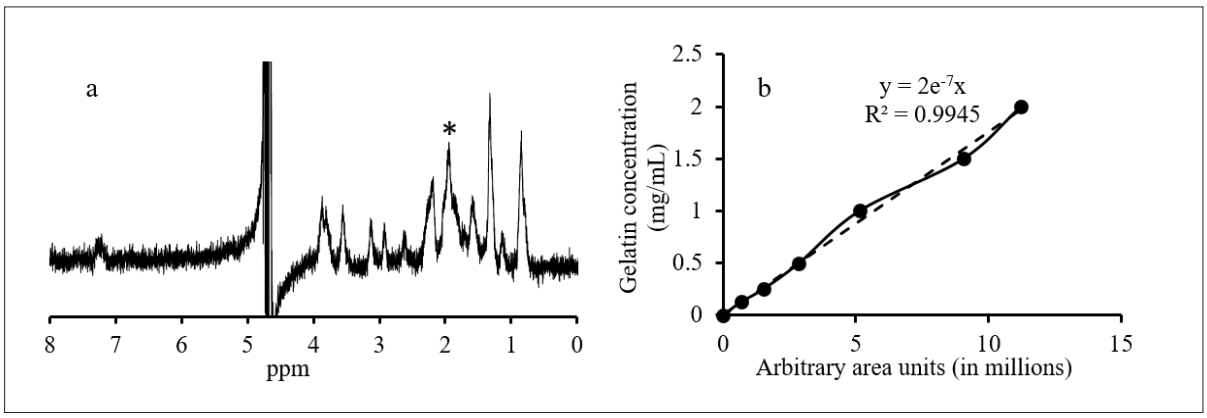


**Figure 2**. (a) NMR spectra of gelatin with characteristic peak at ~1.9 ppm (indicated by *) that was considered for area; (b) gelatin standard curve plotted based on the area corresponding to the gelatin concentration.

and averaged for known quantity of gelatin concentration to obtain a gelatin standard curve as shown in Figure 2b.

### 2.9. Cell viability

The ASC viability was evaluated using a Live/Dead viability kit (ref. L3224, Carlsbad, CA, USA). Briefly, 20 µL of ethidium homodimer-1 and 5 µL of calcein were pipetted into 10 mL of PBS to create the Live/Dead reagent. At specific time points, scaffolds were washed twice with PBS and soaked in 1 mL of reagent solution for at least 30 min under dark conditions at room temperature before imaging under a confocal microscope (Nikon A1R-HD Eclipse Ti2, Melville, NY, USA). A random 5 × 5 $mm^2$ area was imaged with a 40 µm step for each of the three scaffolds at different time points. To quantify the viability results, a maximum intensity projection image was created with red, green, and blue channels using ImageJ software. The red and green channels of the image provided the dead cell and live cell counts. ASC viability in percentage was calculated using this formula: [live cells/(live cells + dead cells)] × 100%.

### 2.10. Statistical analysis

Six samples in each set were used for tensile tests, and three samples in each set were used for cell viability quantification. The results were reported as average ± standard deviation. Minitab® software was used to analyze the difference in means of different groups using one-way analysis of variance (ANOVA). The means were considered significantly different if the *P*-value is less than 0.05.

## 3. Results and discussion

### 3.1. Rheological assessment of hydrogels

One of the objectives of the study was to evaluate the extent of rheological modification of the AG hydrogel with the addition of B3 glass. Hydrogel viscosity and its shear-thinning behavior are crucial in extrusion-based 3D printing processes as such behavior allows the material to flow through the nozzle at low air pressure without causing severe damage to cells. DI water was used to investigate the rheological behavior of B3 glass-mixed gels instead of complete culture media. The reason for this choice is to analyze the true nature of the effect of the dissolved glass and released ions ($Ca^{2+}$, $Mg^{2+}$, and others from the glass) without having any interactions with other salts present in the culture media. It was hypothesized that the effect of B3 glass amount on rheological behavior would serve as a realistic indicator while using gels made with culture media. Despite the evidence in literature demonstrating a significant difference in the swelling of gels made with DI water compared to that of gels made with culture media, the difference is insignificant for viscosity of gels made with DI water or culture media with highly resorbable B3 glass.[36] It was noticed in our experiments that B3 glass dissolves in a few minutes during the gel mixing process to significantly affect gel viscosity irrespective of the media (DI water or culture media). Figure 3 shows the change in viscosity of all hydrogels considered in this study with increasing shear rate. The viscosity of alginate (Alg),

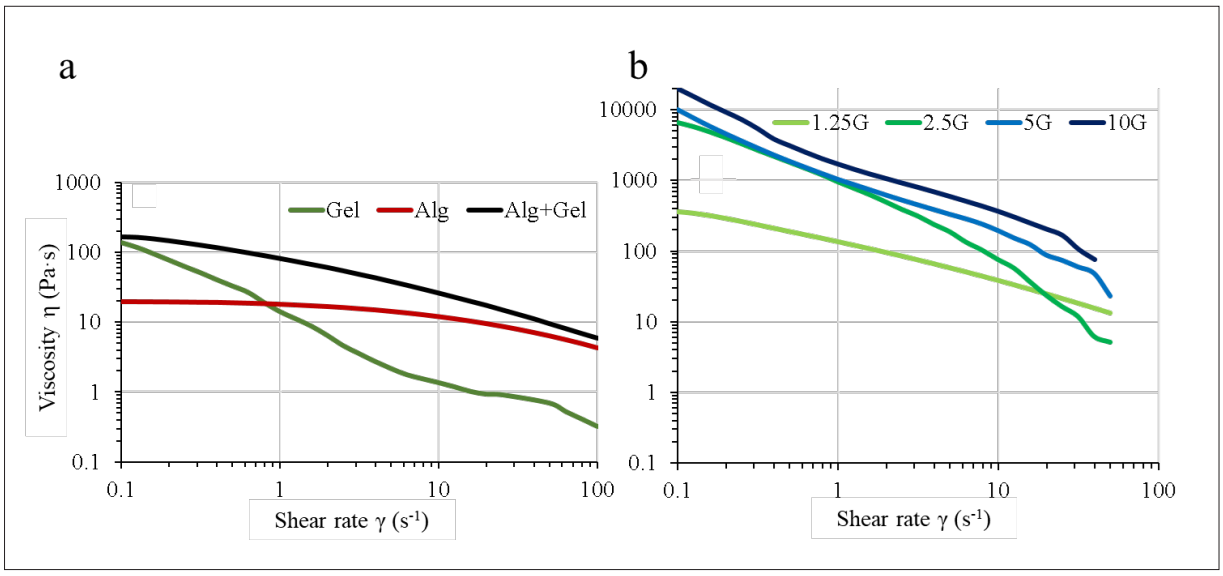


**Figure 3**. Hydrogel viscosity as a function of shear rate at room temperature before crosslinking with $CaCl_2$. (a) Alginate, gelatin, and alginate+gelatin (AG) without glass; (b) effect of B3 glass addition on AG hydrogels in different weight concentrations.

gelatin (Gel), and alginate+gelatin (Alg+Gel or AG) is shown in Figure 3a, and the viscosity of B3 glass-modified AG hydrogels with 1.25 wt.% (1.25G), 2.5 wt.% (2.5G), 5 wt.% (5G), and 10 wt.% (10G) glass content is shown in Figure 3b. The viscosity for all hydrogels was measured at room temperature and before crosslinking with 0.1 M $CaCl_2$ solution. At higher shear rates, modified hydrogels with B3 glass slipped out of the plates (especially, 5G and 10G) of the rheometer, and the test was stopped before the programmed shear rate of 100 $s^{-1}$. Overall, all AG hydrogels irrespective of B3 glass addition showed a shear-thinning behavior with decreased viscosity at increasing shear rates.

As B3 glass is a fast-dissolving bioactive glass, it quickly starts to release $Ca^{2+}$ and $Mg^{2+}$ ions, which are divalent, and other ions including $K^+$, $PO_4^{3-}$, $Na^+$, and $B^{3+}$ to the surrounding aqueous media. As the divalent ions initiate the crosslinking with alginate in the hydrogel, the viscosity of hydrogels with B3 glass was significantly increased by several orders of magnitude (Figure 3b). The addition of 2.5 wt.% B3 glass resulted in a significant and sharp increase in hydrogel viscosity from 1.25 wt.% B3 glass addition (from ~350 Pa·s to ~7000 Pa·s at 100 $s^{-1}$). The differences in viscosity at $t = 0$ s observed for 2.5G, 5G, and 10G hydrogels (~7000 Pa·s, ~10,000 Pa·s, and ~11,000 Pa·s at 100 $s^{-1}$, respectively) were not as significant as viscosity differences between 1.25G and 2.5G hydrogels. These findings suggest the likelihood of an optimal B3 glass concentration, ranging between 1.25 and 2.5 wt.%, for AG hydrogels composed of 3 w/v % alginate and 3 w/v % gelatin.

Amplitude sweep oscillatory tests were conducted on all samples to determine the viscoelastic behavior of AG hydrogels modified with B3 glass. Figure 4 shows the variation of G' and G" with strain percentage and the linear viscoelastic region for each hydrogel. At low concentrations of glass (1.25%), there is no significant difference in the storage modulus (G') in comparison to AG hydrogel (Figure 4b), whereas with the increase in glass concentration to 2.5% made a significant difference. Figure 4c shows the variation in loss modulus (G") for all gels investigated in this study. The transition from G">G' to G'>G" was more prominent in 2.5G, 5G (shown in Figure 4d and e), and 10G hydrogels clearly showing a viscoelastic solid-like behavior with a consistent behavior of G'>G", indicating the increased stiffness of the modified AG hydrogels with B3 glass. This is observed with a clearly defined yield point (cross-over point of G' and G"). The shear stress values around the yield point for gels were recorded as ~3400 Pa for 2.5G, ~3000 Pa for 5G, and ~1300 Pa for 10G. It is also observed that the yield point occurs at lower strain for gels made with higher glass percentage. This seems to be consistent with the lower shear stress values. This could be because of the non-uniformity of the composite AG gels made with higher glass percentages. Figure 4a shows the physical behavior of gels prepared with increasing glass content. It can be clearly seen that gel made with the most glass content behaves like a large piece of crosslinked gel. For example, extruding or manual separation of 10G gel resulted in pockets of crosslinked gel (pockets of gel chunks) being extruded or separated from the hydrogel rather than a single continuous filament extrusion. This non-uniformity is believed to arise during the gel preparation process as pockets of alginate could be crosslinked in a localized manner even before the complete uniform mixing of hydrogel. As a result, during the oscillatory sweep tests, chunks of gels were noticed to break apart and come out of the plates at higher strain.

In addition to shear-thinning and solid-like behavior of hydrogels, the viscosity recovery of the hydrogel after removal of shear force is crucial in extrusion-based 3D bioprinting applications. As hydrogel is extruded through the nozzle, it suffers from higher shear stress and flows through the tip because of a shear-thinning behavior. After deposition of a filament, the hydrogel should recover its molecular structure and viscosity to avoid spreading on the substrate and withstand the weight of successive filaments that would be deposited on top of the current filament. To determine the recovery behavior of B3 glass-modified AG hydrogels in a rheometer, hydrogels were initially maintained under a steady-state shear rate of 0.1 $s^{-1}$ to obtain a stabilized viscosity value. After reaching a steady-state viscosity, the shear rate was increased to higher shear rates (10 $s^{-1}$ and 100 $s^{-1}$) in two separate tests for a specific amount of time (30 s and 10 s, respectively), immediately followed by a cooling period of 0.1 $s^{-1}$ shear rate. Viscosity of hydrogels recorded at different shear rates with time is shown in Figure 5. The recovery data of two tests (at 10 $s^{-1}$ and at 100 $s^{-1}$ shear rates) were combined, and the time scale was adjusted for a simplified representation. A significant drop in viscosity for all hydrogels at increased shear rates can be clearly observed in Figure 5. Recovery time is defined as the time taken for a hydrogel to attain its original steady-state viscosity value from the reduced values at higher shear rates. The shear rate of 100 $s^{-1}$ was used to mimic the behavior of the hydrogel passing through the nozzle tip during extrusion. The results indicated a "near-zero" recovery time for 2.5G and 5G hydrogels after application of 100 $s^{-1}$ shear rate, which was evident from their step-function-like recovery to attain a constant viscosity at 160 s, as shown in Figure 5. 1.25G and AG hydrogels required 60 s and 90 s, respectively, to recover and attain a constant viscosity, as can be observed from the curvature indicated by arrows in Figure 5. It was also observed that hydrogels never truly recovered to 100% of their original steady-state viscosity values (at $t = 0$ s) after the removal

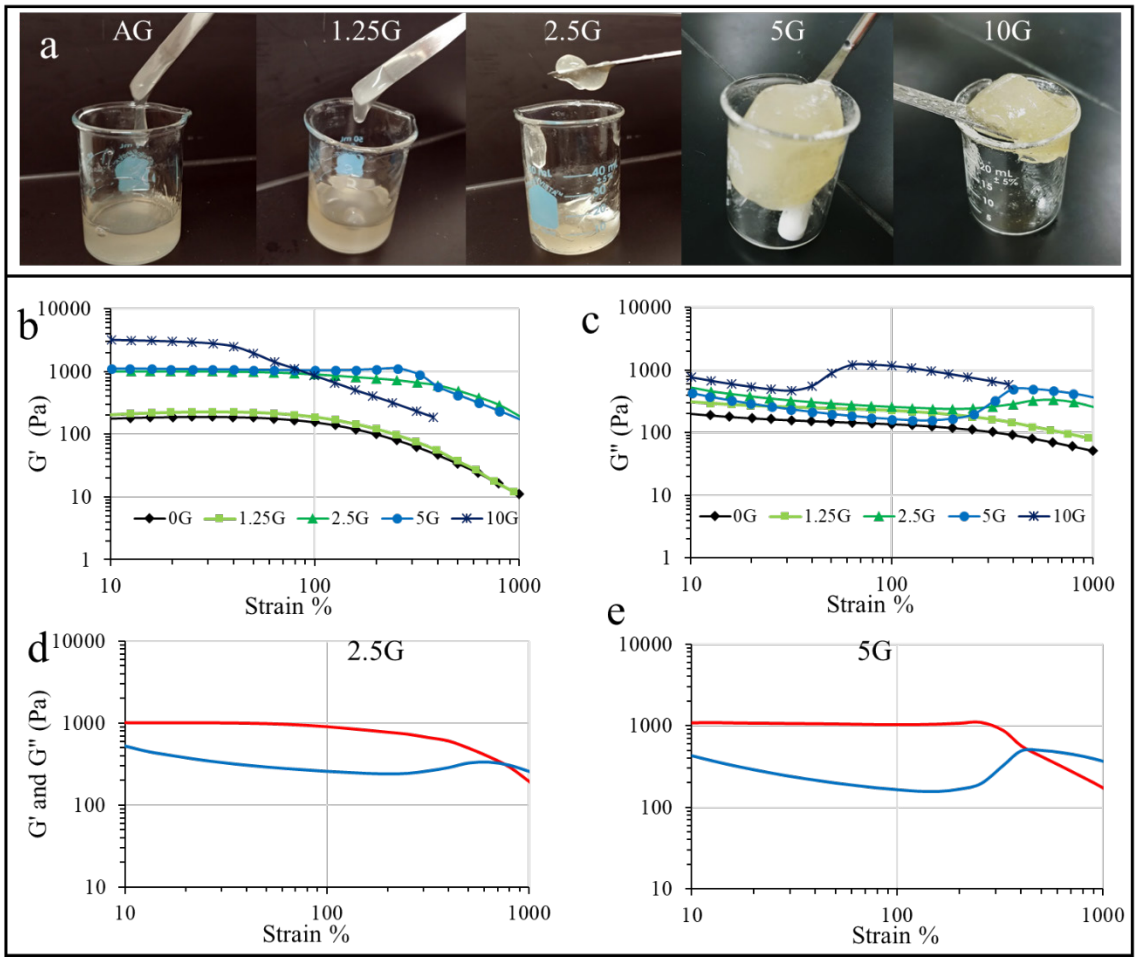


**Figure 4**. Viscoelastic behavior of AG hydrogels. (a) The physical behavior of hydrogels immediately after overnight stirring in a beaker kept on a 40°C hot plate. Flowability of hydrogels stopped with increased B3 glass content (at 2.5G). 2.5G, 5G, and 10G hydrogels exhibit a solid-like behavior. (b) Storage modulus (G') and (c) loss modulus (G") as a function of Strain percentage at room temperature before crosslinking with $CaCl_2$ for alginate-gelatin gels without glass and with different B3 glass weight percentages. (d) G' and G" for 2.5G, and (e) G' and G" for 5G.

of 100 $s^{-1}$ shear rate. For example, steady-state viscosity of 2.5G hydrogel at $t$ = 0 s was ~7000 Pa·s, and its recovered viscosity value between 160 and 220 s was at ~2000 Pa·s. This behavior was noticed in hydrogels with high B3 glass content (>2.5 wt.%) and believed to have occurred due to the loss of material between plates during tests at shear rate of 100 $s^{-1}$. The recovery time results provided a satisfactory representation of the recovery behavior as they confirmed the printability of all hydrogels with and without B3 glass addition. The recovery behavior of 10G hydrogel is not shown in Figure 5 because of its inhomogeneity and high material loss during recovery tests even at low shear rates.

### 3.2. Fabrication, swelling, and mechanical property assessment

The determination of viscosity and material recovery times enabled scaffold fabrication with AG, 1.25G, and 2.5G hydrogels. Six-layered scaffolds measuring 15 × 15 × 1 $mm^3$ were fabricated. The printing parameters used to fabricate scaffolds along with the printability matrix for different hydrogels are shown in Table 1. Hydrogels were first tested for their extrudability through a syringe at different air pressures with different nozzle tips. Although all hydrogel types were extrudable using different tip sizes ranging from internal diameter of 250 μm to 580 μm, the extrusion of highly viscous 5G and 10G hydrogels required high air pressures, extrudate was uneven, and consistent filament formation was not feasible. In part, this could be due to inhomogeneous mixture of alginate and gelatin components in 5G and 10G hydrogels. Addition of more glass meant availability of more $Ca^{2+}$ ions to initiate alginate crosslinking before achieving a homogeneous composite hydrogel. Moreover, utilizing higher air pressures would damage the cells in the hydrogel, and large

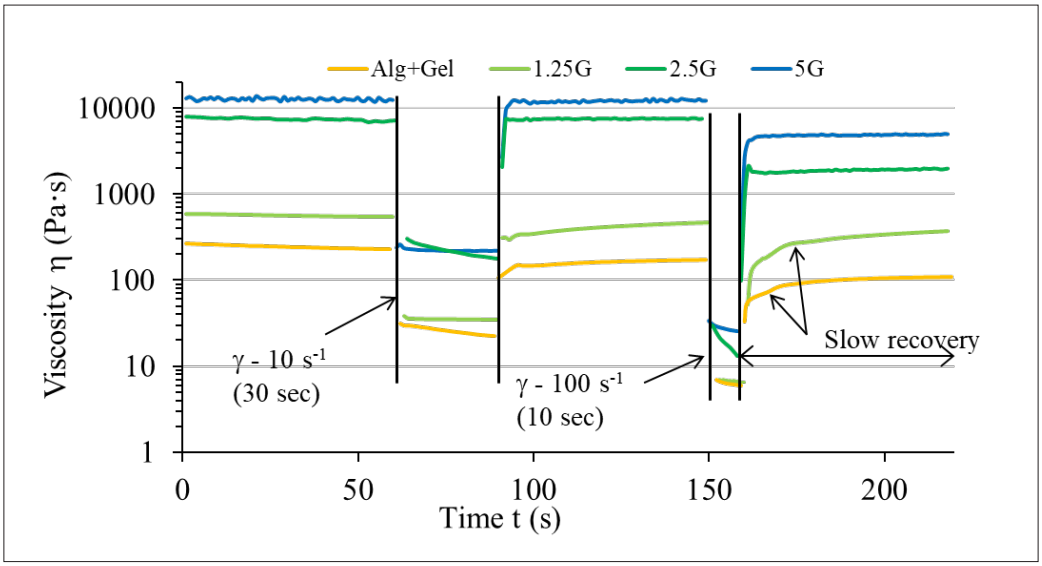


**Figure 5**. Effect of B3 glass addition on the recovery behavior of hydrogels. AG hydrogel and 1.25G required 90 s and 60 s, respectively, to recover to their original viscosity values, whereas 2.5G and 5G show immediate recovery.

tip sizes would compromise the resolution of the fabricated parts. Therefore, by considering the above, scaffolds were fabricated only with AG, 1.25G, and 2.5G hydrogels. Both 22G (410 µm inner diameter) and 25G (250 µm inner diameter) conical-shaped nozzle tips were considered for printing the AG, 1.25G, and 2.5G hydrogels. Specifically, 25G tips were used for AG and 1.25G gels, whereas 22G tip was used for 2.5G gels due to viscosity differences (orders of magnitude different). Despite using a larger tip, the air pressure required to extrude 2.5G gel was four times that of 1.25G, and the extrudate was thinner than that of 1.25G gel. Therefore, the layer height had to be reduced to 0.12 mm from 0.14 mm for AG and 1.25G gels. For AG and 1.25 gels, the extrudate requires time to recover, and therefore despite using a smaller nozzle tip (25G–250 µm), the extrudate spreads immediately after printing and a ~1 mm extrudate was obtained. This spreading behavior is expected based on the viscosity and poor recovery of the AG and 1.25 gels as discussed in our rheological study. A similar sized extrudate (~1 mm) width was obtained for 2.5G gel printed with a larger tip (22G–410 µm) and a much higher air pressure. The recovery time determined by recovery tests was implemented as dwell (wait) time between successive layers during scaffold fabrication. Figure 6 shows scaffolds fabricated before and after dwell time implementation. Before dwell time implementation, fabrication of a designed porous scaffold resulted in solid part formation after six layers of deposition as shown in Figure 6. This happened as the initially deposited layers merged on the substrate unable to recover and carry the weight of successive layers that were deposited during part fabrication. However, dwell time implementation allowed

**Table 1. Scaffold fabrication parameters and printability matrix**

| Fabrication parameters | | | | Printability matrix | | |
|---|---|---|---|---|---|---|
| Hydrogel | AG | 1.25G | 2.5G | Hydrogel | 3D part printability | Filament formation |
| P (psi) | 4 | 5 | 20 | AG | ✓ | ✓ |
| S (mm/s) | 15 | 15 | 15 | 1.25G | ✓ | ✓ |
| h (mm) | 0.14 | 0.14 | 0.12 | 2.5G | ✓ | ✓ |
| t (s) | 90 | 60 | 0 | 5G | × | ~ |
| φ (µm) | 250 | 250 | 410 | 10G | × | ~ |

Abbreviations: P—air pressure; S—table speed; h—layer height; t—wait time between layers; φ—nozzle tip internal diameter; ✓—feasible; ×—not feasible; ~—irregular and inconsistent filament formation.

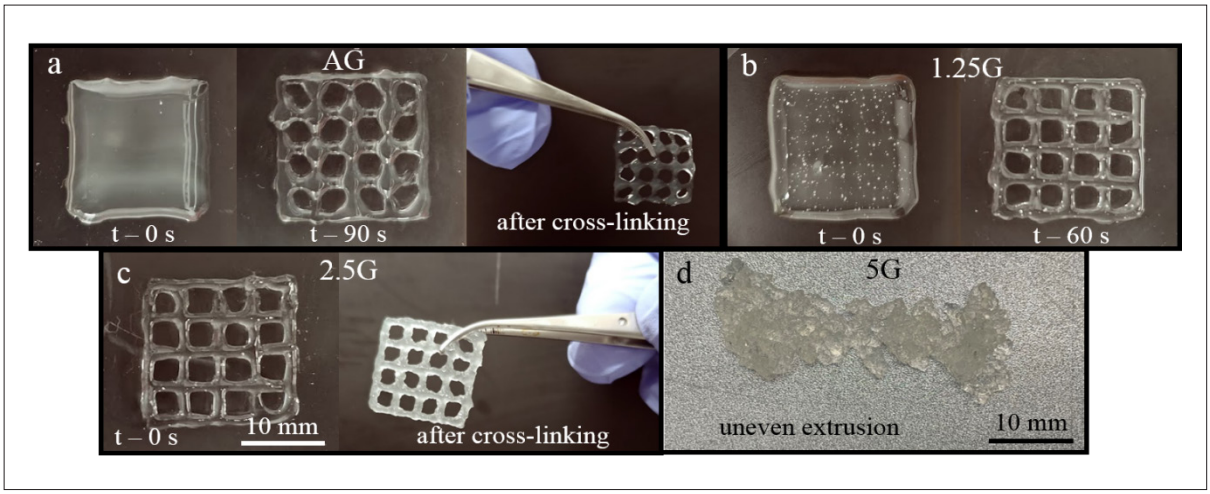


**Figure 6**. Scaffold fabrication with (a) AG, (b) 1.25G, (c) 2.5G, and (d) 5G hydrogels. Implementation of dwell time (t) between successive layer depositions aided in hydrogel recovery and made it feasible to fabricate AG and 1.25G scaffolds. Increasing the B3 glass content reduced the dwell time from 90 s to 0 s as 2.5G hydrogel scaffold could be fabricated with no dwell time. Failure to fabricate parts (dog-bone like specimen) with 5G hydrogel is also shown.

the filament recovery and thus enabled the designed scaffold fabrication. This was further tested in a complex 3D structure with internal channels mimicking a vascular network (Figure 7).

Scaffolds were crosslinked with 0.1 M $CaCl_2$ solution for 10 min immediately after fabrication, washed, and soaked in DI water for 24 h to measure the swelling percentage. Swelling of hydrogels indirectly represents the capacity of the material to absorb media and allow cell growth and proliferation. Swelling of AG hydrogel was increased after 24 h with the addition of B3 glass. The swelling of AG scaffolds was ~36%, whereas it increased to ~44% for 1.25G scaffolds and further to ~51% for 2.5G scaffolds. The release of $Ca^{2+}$ and $Mg^{2+}$ ions with B3 glass dissolution initiates alginate crosslinking during hydrogel preparation (overnight stirring), and the molecular structure was further condensed after crosslinking with $CaCl_2$ solution. Therefore, 2.5G scaffolds have a highly defined and consolidated molecular structure among the three scaffolds, and this was evident from the shrinkage of 2.5G scaffolds (~18%) after crosslinking. After scaffolds were soaked in DI water, they relaxed and absorbed DI water driven by the ionic concentration gradient with high number of ions present inside the scaffold structure (because of glass dissolution), and no ions present in the soaked media (DI water). Hydrogel swelling depends on the ionic concentration of the soaking solution and the number of ionic groups present in the hydrogel. It was reported that increased ionic groups in hydrogel increased its swelling ratio because of the osmotic pressure created by the increased counterions in the hydrogel.[37] This could be the reason for the high swelling percentage observed for 2.5G scaffolds. Higher swelling ratio for AG hydrogels prepared with high ionic strength PBS was also reported in a recent work and was consistent with our results.[13]

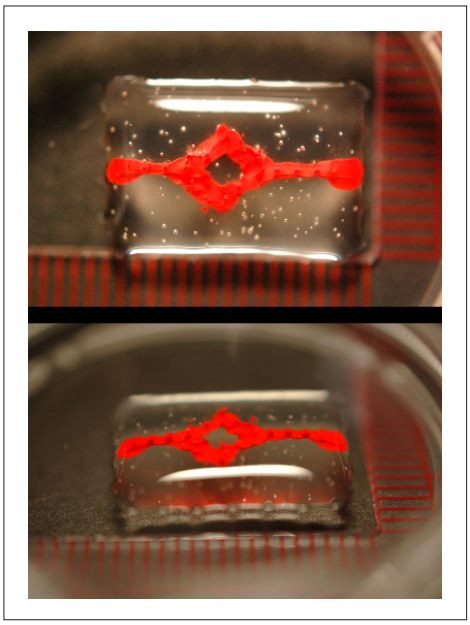

**Figure 7**. A superior (top picture) and anterior (bottom picture) view of a complex structure fabricated by 3D extrusion printing of AG hydrogel-B3 glass composite. A second nozzle was used to extrude red dye to view the internal channel. This construct demonstrates our technique of 3D printing with two different inks.

In this study, small amounts of B3 glass (7.5 mg/10 mL of DI water for 1.25G and 15 mg/10 mL of DI water

for 2.5G) were added to modify the AG hydrogel. The dissolution rate of borate-based glasses including B3 glass in different forms such as glass microspheres, large particles (>200 μm), and scaffolds in DI water, PBS, and simulated body fluid (SBF) have been investigated in the past.[38-41] These studies reported that the majority of B3 glass dissolution occurred during the first 24-h soak period after which the dissolution rate slowed due to the ionic concentration gradient and other factors. In comparison, the glass particles used in the current study are significantly smaller with an average particle size of 3 μm (20 μm mesh sieved) that could have dissolved within 24 h. Therefore, it could be safely assumed that the rheological, swelling, and mechanical properties of the modified AG hydrogels are mostly dependent on the ionic dissolution products of B3 glass and not the physical presence of glass particulates. Figure 8a shows the microstructure of the 2.5G hydrogel, indicating a highly porous and honeycomb-like structure with interconnected porosity. B3 glass particles were not detected in the microstructure, and the characteristic amorphous peaks of the glasses were also absent in the XRD analysis of the 2.5G hydrogel.

Figure 8b shows the dog-bone-shaped specimens utilized for evaluating the tensile strength of hydrogels immediately after crosslinking. A typical load vs. deflection curve for all three specimens is shown in Figure 8c, which indicates the increase in scaffold stiffness with the addition of B3 glass. The elastic modulus of AG, 1.25G, and 2.5G specimens was 33 ± 17 kPa, 62 ± 7 kPa, and 73 ± 13 kPa, respectively, and the ultimate tensile strength of specimens was 26 ± 5 kPa, 21 ± 4 kPa, and 34 ± 9 kPa. 2.5G specimens had highest ultimate tensile strength and were significantly stiffer ($p < 0.05$) in comparison to AG specimens. The increased stiffness was in agreement with the rheological data that showed increased viscosity, decreased recovery time, and a viscoelastic solid-like behavior for 2.5G hydrogels. As the added B3 glass dissolves, the dissolution ions crosslink more alginate polymer chains in the AG hydrogel that causes increased stiffness. Researchers have previously reported that human mesenchymal stem cells (MSCs) encapsulated in ionically crosslinked alginate hydrogels show adipogenic differentiation at moduli of <10 kPa and show osteogenic differentiation at moduli of 11–30 kPa.[42,43] The authors also suggest that osteogenic differentiation of MSCs could be enhanced in hydrogels with faster stress relaxation. AG hydrogels modified with B3 glass (2.5G and 1.25G) have elastic moduli in similar range, and the stress relaxation occurs through breakage and subsequent forming of ionic crosslinks. In addition, stress relaxation could also occur because of the fast swelling of B3 glass modified AG hydrogels (especially, 2.5G). Therefore, the addition of B3 glass to modify AG hydrogels could be useful to tune the human stem cells activity.

An important factor to consider is the retention of scaffold mechanical properties (or scaffold integrity and structure) in culture conditions with time. AG hydrogel strength greatly depends on the w/v % of the alginate and gelatin used in the preparation and the ionic strength of the crosslinking solution. For example, Duan et al. used 6 w/v % of alginate and gelatin (compared to 3 w/v % used in our study), and the crosslinked samples with 0.3 M $CaCl_2$ (compared to 0.1 M $CaCl_2$ in our study) reported improved mechanical properties that were able to sustain for up to 7 days in culture conditions.[14] Our attempts to test specimens after soaking them in DMEM for 7 days at culture conditions were not successful as specimens were broken in the grips of the Instron machine, and insignificant elastic modulus and strength values were recorded. Our results indicated a rapid loss of modulus and strength to a point where they were not suitable for any load-bearing applications, which is in agreement with results reported by Giuseppe et al.[10] However, it must be noted that 1.25G and 2.5G scaffolds had sufficient integrity

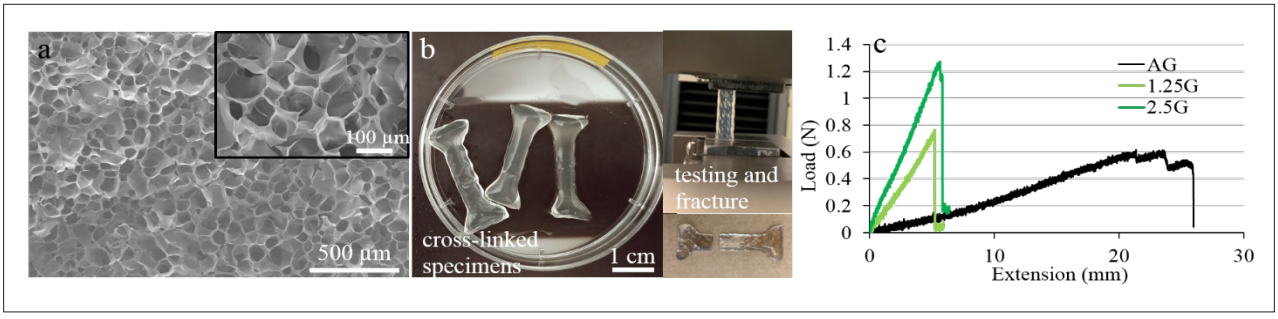


**Figure 8**. (a) SEM image of 2.5G hydrogel with ~100 μm interconnected pores shown in the magnified inlet picture; b) dog-bone specimens used for tensile tests; (c) typical load vs. extension graphs of AG, 1.25G, and 2.5G specimens.

after 14 days in culture to handle and perform biological assays. In general, hydrogel degradation depends on the soaking media composition and enzymes present in it. In our study, DI water was utilized to prepare all hydrogels and to investigate the scaffold swelling characteristics, which are different from other studies where PBS or DMEM was utilized. Nevertheless, samples used for mechanical tests were stored in DMEM to mimic the *in vitro* environment. In addition, we also investigated the structural integrity of 2.5G scaffolds in the CCM at culture conditions without crosslinking with $CaCl_2$ solution. This test was performed to examine if the divalent cations ($Ca^{2+}$ and $Mg^{2+}$) that are released from B3 glass into the hydrogel, which helps initiate the hydrogel crosslinking, would be sufficient to sustain the scaffold structural integrity in culture conditions. Figure 9 shows a collapsed 2.5G scaffold that was not crosslinked after a 2-h incubation in CCM at 37°C, whereas a scaffold crosslinked with 0.1 M $CaCl_2$ retained its structural fidelity after 7 days in culture. This result demonstrates that despite the improvement achieved with B3 glass addition in terms of printability of AG hydrogel, rheological characteristics, and initial mechanical properties, addition of glass alone would not be sufficient to fabricate a 3D scaffold without the chemical crosslinking using $CaCl_2$ solution.

### 3.3. Effect of B3 glass on ASCs viability

One important objective of this study was to evaluate the amount of B3 glass that is acceptable to add to the AG hydrogel to provide viable human ASCs. As B3 glass dissolves much faster than traditional silicate-based bioactive glasses and faster than 45S5 glass, it was important to establish that the resultant concentration of ionic dissolution products has no toxic effects on ASCs *in vitro*. The toxicity could be resulted due to pH increase as alkali ions are released to CCM with B3 glass dissolution. Recently, B3 glass was added to ASCs in two different approaches: directly being added as particles during cell culture, and indirectly (glass dissolution products) exposing cells to two-dimensional (2D) cell culture environment at a B3 glass concentrations that are less than 10 mg/mL.[30,35] These studies reported that a high concentration of B3 glass exposure (>10 mg/mL) could be toxic to ASCs, whereas low concentrations alter ASC protein secretions that may regulate wound healing. Several studies have investigated the toxicity of silicate-based bioactive glasses toward stem cells in a 2D environment, reporting that an optimum concentration of ionic dissolution products could exist upon which the treatment that could be toxic to cells was administered.[44-46] To establish a baseline, we first investigated the B3 glass toxicity to ASCs in 3D environment by adding glass in different weight percentages to AG hydrogel. First, ASCs were encapsulated in AG, 1.25G, 2.5G, 5G, and 10G hydrogels, and 3D-bioprinted as spheroids. To investigate the cell viability, spheroids were cultured in both static (6-well plates under standard culture conditions) and dynamic (6-well plates kept on a rocker) conditions. Figure 10 shows the live/dead assay images of the spheroids on day 0 (2 to 4 h after extrusion and crosslinking), day 1, and day 4 after culture. Spheroids made with 5G and 10G spheroids were irregular in shape because of the high viscosity, and difficulties were encountered to uniformly mix ASCs in these hydrogels. Patches of the hydrogel with empty pockets (without cells) and irregular shapes could be observed in the live/dead images of 5G and 10G hydrogels (Figure 10d, e, i, and n). Also, significant number of dead cells (red spots) can be observed in the live/dead images of 5G and 10G spheroids at all time points which was not the case with other spheroids, whereas more viable ASCs than dead cells were noticed in AG, 1.25G, and 2.5G spheroids.

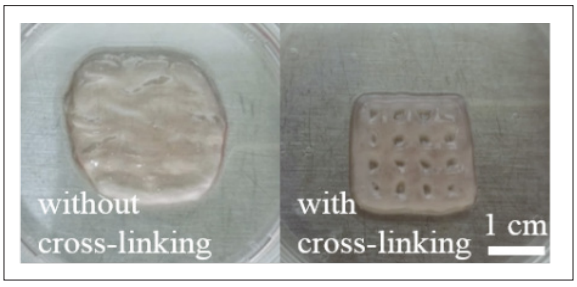


**Figure 9**. 2.5G scaffold in CCM at 37°C after 2 h (left) and after 7 days (right).

Figure 11 shows the quantification of the live/dead assay results. The results clearly indicate that increasing the percentage of B3 glass could be toxic to ASCs in the hydrogel. The viability of ASCs in AG spheroids without B3 glass was significantly higher than ASC viability in 10G, 5G, and 2.5G spheroids immediately after extrusion and crosslinking with $CaCl_2$. ASC viability in spheroids cultured under dynamic conditions was also higher in comparison to viability in spheroids cultured under static conditions after 24 h. This could be due to efficient nutrient transfer to ASCs under dynamic conditions than static conditions. In addition, for spheroids containing B3 glass, $Ca^{2+}$, $B^{3+}$, and other ions released after glass dissolution in the spheroid could diffuse more freely to the media under dynamic conditions than static culture conditions. This could cause the pH of the spheroid to go basic in static conditions and negatively affect ASCs. Addition of B3 glass increased the pH of hydrogels from neutral for AG to pH 8 for 1.25G, pH 8.5 for 2.5G, and up to pH 9 for 10G hydrogel. This could be the reason for high toxicity of B3 glass to ASCs, especially in 2.5G, 5G, and 10G spheroids on day 0, i.e., immediately after mixing ASCs. Though the inside of spheroid maintained relatively high pH, the pH of the surrounding CCM remained neutral during culture

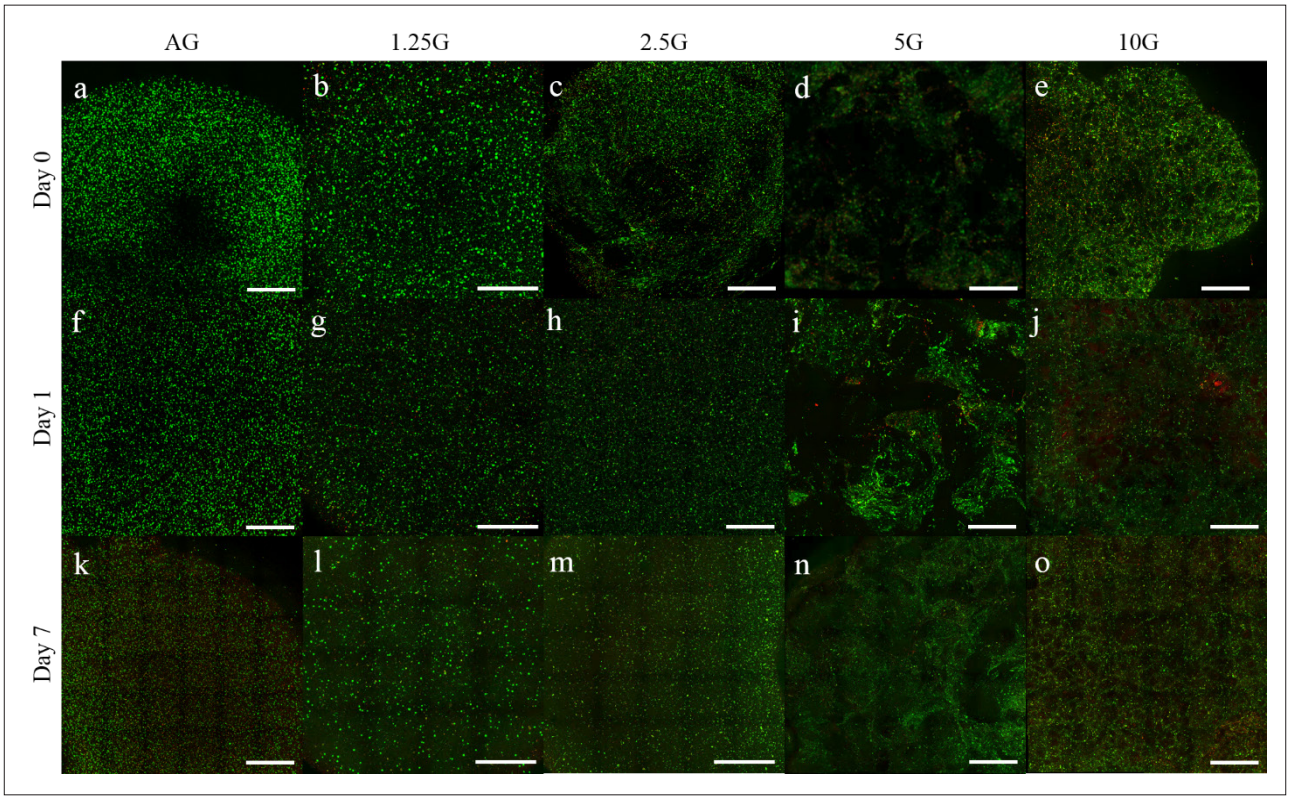


**Figure 10**. Live/Dead assay images of AG, 1.25G, 2.5G, 5G, and 10G spheroids cultured in dynamic conditions for up to 7 days. (a–e) Viability on day 0 (within 2 to 4 h after extrusion), (f–j) viability after 24 h, (k–o) viability after 7 days. Scale bars: 1 mm. Green dots in images represent live cells, and red dots represent dead cells. Undissolved borate glass particles could react with assay reagents and potentially cause green background fluorescence for samples with higher percentage glass (5G and 10G).[26] The background was ignored during cell quantification with ImageJ software.

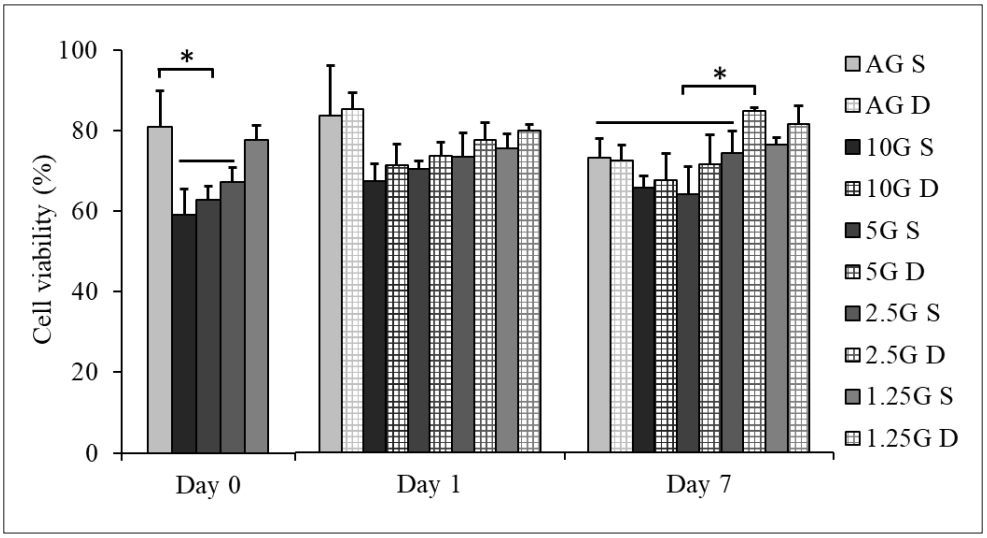


**Figure 11**. ASCs viability in AG, 1.25G, 2.5G, 5G, and 10G spheroids cultured in both static (S; solid columns) and dynamic conditions (D; checkered pattern columns). ASCs viability significantly decreased ($p < 0.05$) with increase in borate glass content (increasing dark shade represents increasing glass content) in less than 4 h after glass addition. ASCs in borate glass-modified hydrogel, which were recovered with time, showed significantly higher viability in hydrogel modified with lower glass percentages ($p < 0.05$).

conditions. This could be attributed to two reasons: (i) the increase in pH due to release of ions from B3 glass to a larger extent could be limited to inside of the hydrogel matrix, and (ii) the release of gelatin from hydrogel matrix to surrounding media could neutralize the increase in pH because of any ions released from B3 glass, thereby causing the pH of the media to remain in the neutral range (7–7.6) for all gel types (1.25G to 10G). In any case, with the regular change in media and presence of dynamic culture conditions, pH of the spheroids and neutralized media as well as ASC viability eventually improved after 7 days in culture, and 2.5G spheroids had significantly higher viability than AG spheroids.

The ASC viability in spheroidal culture helped determine the range of viable B3 glass percentages that could be added to AG hydrogel (0.075 and 0.15 w/v % or 1.25G and 2.5G gels) and the suitable culture conditions (dynamic better than static). Nonetheless, it is important to validate the established B3 glass concentrations and culture conditions with the 3D-printed constructs. Therefore, AG, 1.25G and 2.5G lattice structures containing ASCs and measuring 15 × 15 × 1 $mm^3$ were bioprinted and cultured for up to 7 days under dynamic conditions. Figure 12 shows the live/dead assay images of the scaffolds. A higher percentage of viable ASCs (green spots) than dead cells can be clearly seen in all images. A higher percentage of dead cells in the edges of the pores, possibly caused by the crosslinking with $CaCl_2$ solution, is a notable observation. Figure 13 shows the results of quantified live/dead assay images of bioprinted scaffolds. The ASC viability in scaffolds was similar to the viability of AG, 1.25G, and 2.5G spheroids, with ASC viability in AG scaffold being significantly higher than 2.5G scaffold. However, after 7 days in culture, despite possessing a higher percentage of viable ASC populations, both 1.25G and 2.5G scaffolds were not significantly different than AG scaffolds in terms of cell viability. In addition, a significant decline in ASC viability in AG hydrogel was observed in both bioprinted scaffolds and spheroids from day 1 to day 7 under culture conditions. The decline in ASC viability could be attributed to the release of gelatin from AG hydrogel scaffold. In this study, gelatin was mainly added for cell adhesion and proliferation as alginate alone does not contain the necessary RGD tripeptide to support cell adhesion. In AG

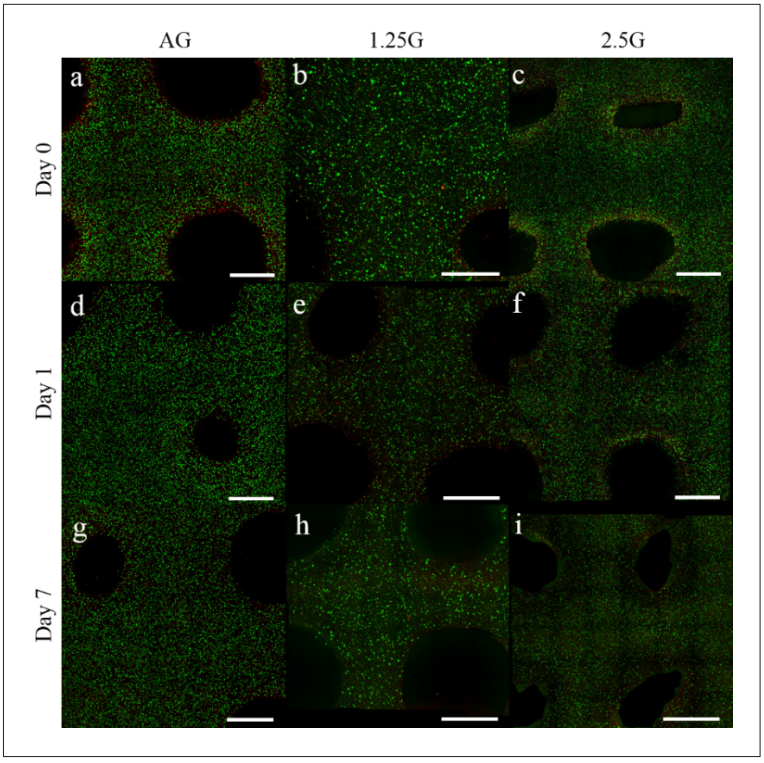


**Figure 12**. Live/Dead assay images of bioprinted AG, 1.25G, and 2.5G scaffolds cultured in dynamic conditions for up to 7 days. (a–c) viability on day 0 (within 2 to 4 h after bioprinting and crosslinking), (d–f) viability after 24 h, and (g–i) viability after 7 days. Scale bars: 1 mm. A higher percentage of dead cells (red spots) were observed near pore edges in comparison with the scaffold interior, indicating cell death due to exposure to $CaCl_2$ solution during crosslinking and the overall presence of low cell numbers at edges.

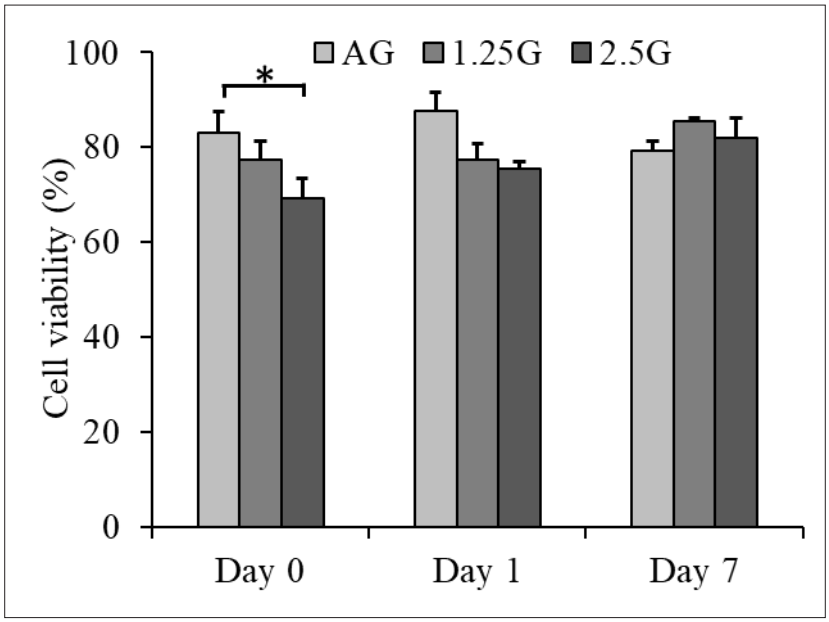


**Figure 13.** ASCs viability in AG, 1.25G, and 2.5G bioprinted scaffolds cultured in dynamic conditions. ASCs viability significantly decreased ($p < 0.05$) with the addition of 2.5 wt.% borate glass content in bioprinted scaffolds in less than 4 h after glass addition. After 7 days in culture, ASCs, which were recovered in modified hydrogels, exhibited higher cell viability in scaffolds bioprinted with modified hydrogels in comparison with AG hydrogel, although the difference was not statistically significant ($p < 0.05$).

hydrogel preparation, gelatin and alginate hydrogels were physically blended together to form a composite hydrogel. In order to study the release of gelatin from the AG hydrogel used in this study, AG, 1.25G and 2.5G scaffolds measuring $15 \times 15 \times 1$ mm$^3$ were fabricated without cells, crosslinked with $CaCl_2$ solution, and soaked in DI water under standard culture conditions for up to 7 days. The surrounding DI water was collected after 24 h and on day 7 and checked for gelatin presence using proton nuclear magnetic resonance ($^1$H-NMR) spectroscopy (Figure 2). The results indicated that gelatin release started immediately after crosslinking and continued as scaffolds incubated in DI water (Figure 14). This loss of ~70% of gelatin from the scaffold could possibly explain the decline in ASC viability after 7 days in culture in AG scaffolds. The release of gelatin from 1.25G and 2.5G scaffolds was ~40% and ~50%, respectively, which could explain the modest improvement in cell viability in these scaffolds in comparison to AG scaffolds after 7 days. A more appropriate possibility in future could be to covalently crosslink the gelatin and alginate molecular chains for prolonged culture conditions and slow down the release of gelatin from the structure (limited to no more than ~25% after 7 days) as proposed in one study.[47]

Studies that have previously investigated the hydrogel+bioactive glass composite focused on creating a 3D porous matrix or scaffolds for cell seeding and injectable matrix for bone repair, as well as applications mostly limited to bone tissue engineering.[48-54] To date, very few studies have investigated the addition of bioactive glass to hydrogel to regulate hydrogel viscosity and incorporate cells in the hydrogel+bioactive glass matrix for bioprinting tissue models or 3D cell culture applications.[55-58] Addition of silicate-based bioactive glass nanoparticles to alginate dialdehyde-gelatin promoted bone-like apatite layer formation and showed no toxicity to the bioprinted human osteosarcoma cells (MG-63).[55] Results from experimenting with human dental pulp stem cells (DPSCs) encapsulated in a bioactive glass containing alginate/Matrigel composite hydrogel indicated higher levels of osteogenic expression by DPSCs in the presence of both Matrigel and bioactive glass.[57] Although bioactive glass composition was not reported in the aforementioned study, the minimal effects on mechanical properties of composite hydrogels could perhaps indicate a slow dissolving silicate-based bioactive glass. In another study, ionic dissolution products of a silicate-based bioactive glass were used to prepare an osteogenic media to culture and crosslink gellan gum or collagen type I hydrogels containing ASCs. Another study reported osteogenesis of ASCs in hydrogels modified with bioactive glass.[58] One common aspect in the above studies is the use of silicate-based bioactive glass. The dissolution rates of silicate-based glasses are several times slower in comparison to borate-based glasses.[15] Therefore, nanoparticles of silicate-based glass are often used to fasten

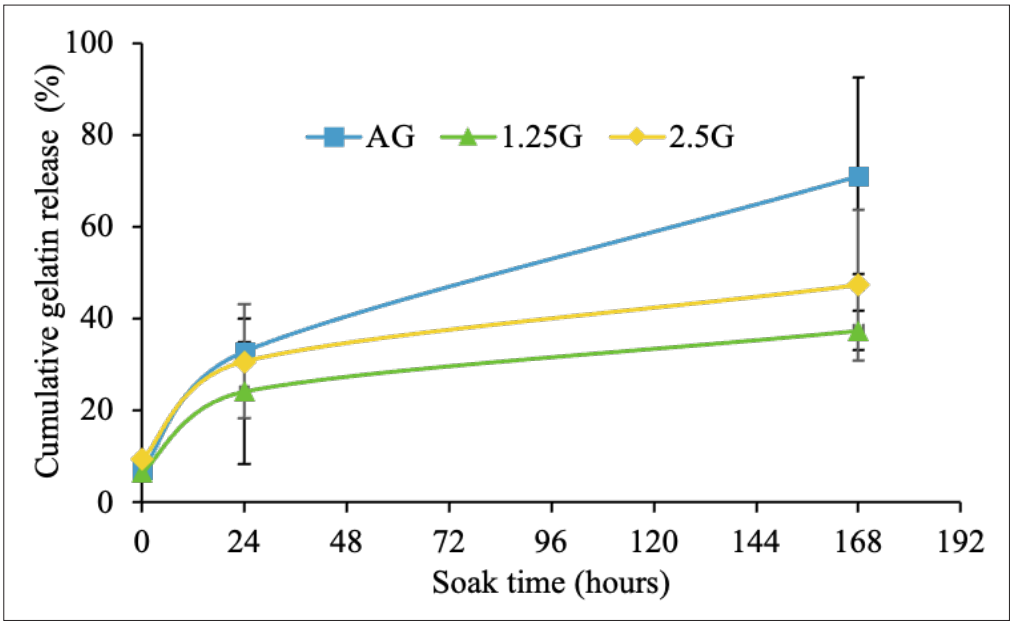


**Figure 14.** Gelatin release profiles from AG, 1.25G, and 2.5G scaffolds.

the glass particle dissolution and release ions to control the hydrogel viscosity and establish a window of printable time for the composite hydrogel.[55] However, borate-based bioactive glasses dissolve rapidly and supply the dissolution products (including $Ca^{2+}$ ions) to control the hydrogels viscosity for 3D printing without affecting their shear-thinning behavior. The mechanisms that are currently adopted during bioprinting with alginate-based hydrogels include filament exposure to $CaCl_2$ solution to initiate crosslinking and fabrication under temperature-controlled environment by modifying the solvent ionic strength.[13,59] In this study, we successfully demonstrated bioprinting with borate glass-modified hydrogels at room temperature. This study is the first to report the use of borate-based bioactive glass to improve the extrudability of alginate-based hydrogels with consideration of human ASC viability.

## 4. Conclusion

Our research showcased the capability of B3 glass to facilitate printing using AG hydrogel at room temperature, eliminating the requirement for a temperature-controlled setting. This improvement was analyzed not just in terms of the hydrogel's printability at room temperature, but also regarding its impact on cell viability. Rheological properties of an AG hydrogel were modified with the addition of 0.075 to 0.6 w/v % of highly resorbable B3 glass, and scaffolds were successfully fabricated. The addition of B3 glass (0.075 and 0.15 w/v %) increased the viscosity (from 0.2 kPa·s to 7 kPa·s) and made the AG hydrogel exhibit a viscoelastic solid-like behavior (G'> G") that improved the hydrogel recovery and enabled effortless extrusion 3D printing of scaffolds. AG scaffold stiffness increased with the addition of B3 (from 33 kPa to 73 kPa), and the mechanical properties showed the potential of the modified AG hydrogel to serve as a viable matrix for human ASCs. Despite the toxicity of B3 to ASCs when added in quantities higher than 0.3 w/v % to hydrogel (<70% viable ASCs), lower quantities of B3 have increased the viability in comparison to AG hydrogels without B3 after 7 days in culture (>80% viable ASCs). Overall, the rheological modification of alginate-based hydrogels with B3 glass showed the potential for future applications in extrusion-based bioprinting with human ASCs.

## Acknowledgments

The authors thank Austin Martin and Jeremy Watts for their help with rheological assessment of hydrogels and freeze-drying hydrogels. The glass used in this study was provided by Mo-Sci Corporation, Rolla, MO, USA.

## Funding

This research was funded by the Intelligent Systems Center and the Center for Biomedical Research at the Missouri University of Science and Technology.

## Conflict of interest

The authors declare no conflicts of interest.

## Author contributions

*Conceptualization:* Krishna C.R. Kolan, Julie A. Semon
*Investigation:* Krishna C.R. Kolan, Lesa B. Steen, August T. Bindbeutel, Apurv Saxena, Bradley A. Bromet
*Methodology:* Krishna C.R. Kolan, Julie A. Semon, Apurv Saxena
*Formal analysis:* Krishna C.R. Kolan, Julie A. Semon
*Writing – original draft:* Krishna C.R. Kolan
*Writing – review & editing:* Apurv Saxena, Delbert E. Day, Julie A. Semon, Ming C. Leu

## Ethics approval and consent to participate

Not applicable.

## Consent for publication

Not applicable.

## Availability of data

The datasets generated during the current study are available from the corresponding author upon reasonable request.

## References


1. Ozbolat IT, Hospodiuk M. Current advances and future perspectives in extrusion-based bioprinting. *Biomaterials*. 2016;76:321-343. doi: 10.1016/j.biomaterials.2015.10.076
2. Choudhury D, Anand S, Naing M. The arrival of commercial bioprinters – towards 3D bioprinting revolution! *Int J Bioprint*. 2018;4(2). doi: 10.18063/IJB.v4i2.139
3. Gungor-Ozkerim PS, Inci I, Zhang YS, Khademhosseini A, Dokmeci MR. Bioinks for 3D bioprinting: an overview. *Biomater Sci*. 2018;6(5):915-946. doi: 10.1039/c7bm00765e
4. Rowley JA, Madlambayan G, Mooney DJ. Alginate hydrogels as synthetic extracellular matrix materials. *Biomaterials*. 1999;20(1):45-53. doi: 10.1016/S0142-9612(98)00107-0
5. Smidsrød O, Skjåk-Braek G. Alginate as immobilization matrix for cells. *Trends Biotechnol*. 1990;8(3):71-78. doi: 10.1016/0167-7799(90)90139-O
6. Reakasame S, Boccaccini AR. Oxidized alginate-based hydrogels for tissue engineering applications: a review. *Biomacromolecules*. 2018;19(1):3-21. doi: 10.1021/acs.biomac.7b01331
7. Jeon O, Alsberg E. Photofunctionalization of alginate hydrogels to promote adhesion and proliferation of human mesenchymal stem cells. *Tissue Eng Part A*. 2013;19(11-12):1424-1432. doi: 10.1089/ten.TEA.2012.0581
8. Alsberg E, Anderson KW, Albeiruti A, Franceschi RT, Mooney DJ. Cell-interactive alginate hydrogels for bone tissue engineering. *J Dent Res*. 2001;80(11):2025-2029. doi: 10.1177/00220345010800111501
9. Rastogi P, Kandasubramanian B. Review of alginate-based hydrogel bioprinting for application in tissue engineering. *Biofabrication*. 2019;11(4):042001. doi: 10.1088/1758-5090/ab331e
10. Giuseppe M Di, Law N, Webb B, et al. Mechanical behaviour of alginate-gelatin hydrogels for 3D bioprinting. *J Mech Behav Biomed Mater*. 2018;79:150-157. doi: 10.1016/J.JMBBM.2017.12.018
11. Chung JHY, Naficy S, Yue Z, et al. Bio-ink properties and printability for extrusion printing living cells. *Biomater Sci*. 2013;1(7):763. doi: 10.1039/c3bm00012e
12. Jiang T, Munguia-Lopez J, Flores-Torres S, et al. Bioprintable alginate/gelatin hydrogel 3D in vitro model systems induce cell spheroid formation. *J Vis Exp*. 2018;(137):e57826. doi: 10.3791/57826
13. Li Z, Huang S, Liu Y, et al. Tuning alginate-gelatin bioink properties by varying solvent and their impact on stem cell behavior. *Sci Rep*. 2018;8(1):8020. doi: 10.1038/s41598-018-26407-3
14. Duan B, Hockaday LA, Kang KH, Butcher JT. 3D Bioprinting of heterogeneous aortic valve conduits with alginate/gelatin hydrogels. *J Biomed Mater Res Part A*. 2013;101A(5):1255-1264. doi: 10.1002/jbm.a.34420
15. Rahaman MN, Day DE, Sonny Bal B, et al. Bioactive glass in tissue engineering. *Acta Biomater*. 2011;7(6):2355-2373. doi: 10.1016/j.actbio.2011.03.016
16. Kokubo T, Takadama H. How useful is SBF in predicting in vivo bone bioactivity? *Biomaterials*. 2006;27(15):2907-2915. doi: 10.1016/j.biomaterials.2006.01.017
17. Miguez-Pacheco V, Hench LL, Boccaccini AR. Bioactive glasses beyond bone and teeth: emerging applications in contact with soft tissues. *Acta Biomater*. 2015;13:1-15. doi: 10.1016/J.ACTBIO.2014.11.004
18. Richard M. *Bioactive Behavior of a Borate Glass*. Master's Theses. Missouri University of Science and Technology; 2000.
19. Jung S. *Borate Based Bioactive Glass Scaffolds for Hard and Soft Tissue Engineering*. Dissertation. Missouri University of Science and Technology; 2010.
20. George J. *Dissolution of Borate Glasses and Precipitation of Phosphate Compounds*. Dissertation. Missouri University of Science and Technology; 2015.
21. Nychka JA, Mazur SLR, Kashyap S, Li D, Yang F. Dissolution of bioactive glasses: the effects of crystallinity coupled with stress. *JOM*. 2009;61(9):45-51.

doi: 10.1007/s11837-009-0132-5

22. Liu X, Rahaman MN, Day DE. Conversion of melt-derived microfibrous borate (13-93B3) and silicate (45S5) bioactive glass in a simulated body fluid. *J Mater Sci Mater Med*. 2013;24(3):583-595. doi: 10.1007/s10856-012-4831-z

23. Zhao F, Yang Z, Xiong H, Yan Y, Chen X, Shao L. A bioactive glass functional hydrogel enhances bone augmentation via synergistic angiogenesis, self-swelling and osteogenesis. *Bioact Mater*. 2023;22:201-210. doi: 10.1016/j.bioactmat.2022.09.007

24. Zhu H, Monavari M, Zheng K, et al. 3D bioprinting of multifunctional dynamic nanocomposite bioinks incorporating Cu-doped mesoporous bioactive glass nanoparticles for bone tissue engineering. *Small*. 2022;18(12):2104996. doi: 10.1002/smll.202104996

25. Monavari M, Homaeigohar S, Medhekar R, et al. A 3D-printed wound-healing material composed of alginate dialdehyde-gelatin incorporating astaxanthin and borate bioactive glass microparticles. *ACS Appl Mater Interfaces*. 2023;15(44):50626-50637. doi: 10.1021/acsami.2c23252

26. Kolan KCR, Semon JA, Bromet B, Day DE, Leu MC. Bioprinting with human stem cells-laden alginate-gelatin bioink and bioactive glass for tissue engineering. *Int J Bioprint*. 2019;5(2.2):3. doi: 10.18063/ijb.v5i2.2.204

27. Jung SB. Borate based bioactive glass scaffolds for hard and soft tissue engineering. *Zhurnal Eksp i Teor Fiz*. 2010;389.

28. Watters R, Brown R, Day D. Angiogenic effect of bioactive borate glass microfibers and beads in the hairless mouse. *Bioact Glas*. 2015;1(1). doi: 10.1515/bglass-2015-0017

29. Lin Y, Brown RF, Jung SB, Day DE. Angiogenic effects of borate glass microfibers in a rodent model. *J Biomed Mater Res Part A*. 2014;102(12):4491-4499. doi: 10.1002/jbm.a.35120

30. Thyparambil N, Gutgesell L, Bromet B, et al. Bioactive borate glass triggers phenotypic changes in adipose stem cells. *J Mater Sci Mater Med*. 2020;31(4):35. doi: 10.1007/s10856-020-06366-w

31. Dykstra JA, Facile T, Patrick RJ, et al. Concise review: fat and furious: harnessing the full potential of adipose-derived stromal vascular fraction. *Stem Cells Transl Med*. 2017;6(4):1096-1108. doi: 10.1002/sctm.16-0337

32. Gimble JM, Guilak F, Bunnell BA. Clinical and preclinical translation of cell-based therapies using adipose tissue-derived cells. *Stem Cell Res Ther*. 2010;1(2):19. doi: 10.1186/scrt19

33. Bourin P, Bunnell BA, Casteilla L, et al. Stromal cells from the adipose tissue-derived stromal vascular fraction and culture expanded adipose tissue-derived stromal/stem cells: a joint statement of the International Federation for Adipose Therapeutics and Science (IFATS) and the International Society for Cellular Therapy (ISCT). *Cytotherapy*. 2013;15(6):641-648. doi: 10.1016/j.jcyt.2013.02.006

34. Kolan KCR, Semon JA, Bindbeutel AT, Day DE, Leu MC. Bioprinting with bioactive glass loaded polylactic acid composite and human adipose stem cells. *Bioprinting*. 2020;18:e00075. doi: 10.1016/j.bprint.2020.e00075

35. Thyparambil NJ, Gutgesell LC, Hurley CC, Flowers LE, Day DE, Semon JA. Adult stem cell response to doped bioactive borate glass. *J Mater Sci Mater Med*. 2020;31(2):1-8. doi: 10.1007/s10856-019-6353-4

36. Suvarnapathaki S, Nguyen MA, Wu X, Nukavarapu SP, Camci-Unal G. Synthesis and characterization of photocrosslinkable hydrogels from bovine skin gelatin. *RSC Adv*. 2019;9:13016-13025. doi: 10.1039/c9ra00655a

37. Okay O. *General Properties of Hydrogels*. Berlin, Heidelberg: Springer; 2009:1-14. doi: 10.1007/978-3-540-75645-3_1

38. Jung S, Day D. Conversion kinetics of silicate, borosilicate, and borate bioactive glasses to hydroxyapatite. *Phys Chem Glas*. 2009;50(2):85-88.

39. Liu X, Pan H, Fu H, Fu Q, Rahaman MN, Huang W. Conversion of borate-based glass scaffold to hydroxyapatite in a dilute phosphate solution. *Biomed Mater*. 2010;5(1):015005. doi: 10.1088/1748-6041/5/1/015005

40. George JL, Brow RK. In-situ characterization of borate glass dissolution kinetics by μ-Raman spectroscopy. *J Non Cryst Solids*. 2015;426:116-124. doi: 10.1016/J.JNONCRYSOL.2015.07.003

41. Fu Q, Rahaman MN, Fu H, Liu X. Silicate, borosilicate, and borate bioactive glass scaffolds with controllable degradation rate for bone tissue engineering applications. I. Preparation and in vitro degradation. *J Biomed Mater Res Part A*. 2010;95A(1):164-171. doi: 10.1002/jbm.a.32824

42. Huebsch N, Arany PR, Mao AS, et al. Harnessing traction-mediated manipulation of the cell/matrix interface to control stem-cell fate. *Nat Mater*. 2010;9(6):518-526. doi: 10.1038/nmat2732

43. Chaudhuri O, Gu L, Klumpers D, et al. Hydrogels with tunable stress relaxation regulate stem cell fate and activity. *Nat Mater*. 2016;15(3):326-334. doi: 10.1038/nmat4489

44. Qazi TH, Hafeez S, Schmidt J, Duda GN, Boccaccini AR, Lippens E. Comparison of the effects of 45S5 and 1393 bioactive glass microparticles on hMSC behavior. *J Biomed Mater Res A*. 2017;105(10):2772-2782. doi: 10.1002/jbm.a.36131

45. Hoppe A, Boccaccini AR. Biological impact of bioactive glasses and their dissolution products. *Front Oral Biol*. 2015;17:22-32. doi: 10.1159/000381690

46. Wang X, Tolba E, Schröder HC, et al. Effect of bioglass on growth and biomineralization of SaOS-2 cells in hydrogel after 3D cell bioprinting. *PLoS One*. 2014;9(11):e112497. doi: 10.1371/journal.pone.0112497

47. Sarker B, Singh R, Silva R, et al. Evaluation of fibroblasts adhesion and proliferation on alginate-gelatin crosslinked hydrogel. *PLoS One*. 2014;9(9):e107952. doi: 10.1371/journal.pone.0107952

48. Couto DS, Hong Z, Mano JF. Development of bioactive and biodegradable chitosan-based injectable systems containing bioactive glass nanoparticles. *Acta Biomater*. 2009;5(1): 115-123. doi: 10.1016/j.actbio.2008.08.006

49. Nikpour P, Salimi-Kenari H, Fahimipour F, et al. Dextran hydrogels incorporated with bioactive glass-ceramic: nanocomposite scaffolds for bone tissue engineering. *Carbohydr Polym*. 2018;190:281-294. doi: 10.1016/j.carbpol.2018.02.083

50. Killion JA, Kehoe S, Geever LM, et al. Hydrogel/bioactive glass composites for bone regeneration applications: synthesis and characterisation. *Mater Sci Eng C*. 2013;33(7):4203-4212. doi: 10.1016/j.msec.2013.06.013

51. Moreira CDF, Carvalho SM, Sousa RG, Mansur HS, Pereira MM. Nanostructured chitosan/gelatin/bioactive glass in situ forming hydrogel composites as a potential injectable matrix for bone tissue engineering. *Mater Chem Phys*. 2018;218:304-316. doi: 10.1016/j.matchemphys.2018.07.039

52. Gantar A, Drnovšek N, Casuso P, et al. Injectable and self-healing dynamic hydrogel containing bioactive glass nanoparticles as a potential biomaterial for bone regeneration. *RSC Adv*. 2016;6(73):69156-69166. doi: 10.1039/C6RA17327F

53. Zhu N, Chatzistavrou X, Papagerakis P, Ge L, Qin M, Wang Y. Silver-doped bioactive glass/chitosan hydrogel with potential application in dental pulp repair. *ACS Biomater Sci Eng*. 2019;5(9):4624-4633. doi: 10.1021/acsbiomaterials.9b00811

54. Washio A, Teshima H, Yokota K, Kitamura C, Tabata Y. Preparation of gelatin hydrogel sponges incorporating bioactive glasses capable for the controlled release of fibroblast growth factor-2. *J Biomater Sci Polym Ed*. 2019;30(1):49-63. doi: 10.1080/09205063.2018.1544474

55. Leite ÁJ, Sarker B, Zehnder T, Silva R, Mano JF, Boccaccini AR. Bioplotting of a bioactive alginate dialdehyde-gelatin composite hydrogel containing bioactive glass nanoparticles. *Biofabrication*. 2016;8(3):035005. doi: 10.1088/1758-5090/8/3/035005

56. Douglas TEL, Dziadek M, Gorodzha S, et al. Novel injectable gellan gum hydrogel composites incorporating Zn- and Sr-enriched bioactive glass microparticles: High-resolution X-ray microcomputed tomography, antibacterial and in vitro testing. *J Tissue Eng Regen Med*. 2018;12(6): 1313-1326. doi: 10.1002/term.2654

57. Sevari SP, Shahnazi F, Chen C, Mitchell JC, Ansari S, Moshaverinia A. Bioactive glass-containing hydrogel delivery system for osteogenic differentiation of human dental pulp stem cells. *J Biomed Mater Res Part A*. 2020;108(3):557-564. doi: 10.1002/jbm.a.36836

58. Vuornos K, Ojansivu M, Koivisto JT, et al. Bioactive glass ions induce efficient osteogenic differentiation of human adipose stem cells encapsulated in gellan gum and collagen type I hydrogels. *Mater Sci Eng C*. 2019;99:905-918. doi: 10.1016/j.msec.2019.02.035

59. Sun W, Starly B, Daly AC, et al. The bioprinting roadmap. *Biofabrication*. 2020;12(2):022002. doi: 10.1088/1758-5090/ab5158